SYNTHETIC EXAMPLES OF PRE-STACK MIGRATION

Jeff Thorson

Introduction

The concept of migration before stack by means of the Double-Square-Root (DSR) equation is well known to the readers of the reports of the Stanford Exploration Project. Using the DSR equation to perform migration before stack, or "shot-geophone" migration, can be seen to be equivalent to a simultaneous downward continuation of common-shot gathers and common-geophone gathers. The purpose of this paper is not a full exposition of the DSR equation -- for this, refer to Claerbout (SEP-15, p.73) and Clayton (SEP-14, p.21) for an analysis of the equation and the physical interpretation in terms of downward continuation. Instead, this paper discusses the practical implementation of the DSR equation in performing pre-stack migration, summarizing the important concepts along the way.

Concepts

Shot-geophone migration is the procedure which operates on an entire set of field data -- all shot gathers of a single line -- to produce a correctly imaged section. Now the "field data" may be organized into a three-dimensional dataset, indexed by shot coordinate s, geophone coordinate g, and time sample t. Indicate the three-dimensional wave field recorded on the surface (a flat datum z=0) as $u(s,g,t,z=0)$. The prospect of working with the entire dataset of a seismic experiment does not seem particularly inviting. However, the dimensionality of the migration problem may be reduced by a factor of one by

5

working in the time-frequency domain. If each frequency sample is operated on separately, data organization is simpler and storage requirements are more manageable. especially on a minicomputer system such as the one that produced the models in this paper. The amount of computation required for the migration to run to completion is not necessarily less in the frequency domain than in the time domain, but computation time may be shortened by being able to dispense with data transposes and disk transfers required in the time domain.

The Double-Square-Root equation in the frequency domain (Claerbout, 1978) is

$$\frac{\partial u}{\partial z} = \pm i \left\{ \left[\frac{\omega^2}{v^2(s,z)} + \partial_{ss} \right]^{\frac{1}{2}} + \left[\frac{\omega^2}{v^2(g,z)} + \partial_{gg} \right]^{\frac{1}{2}} \right\} u \qquad (1)$$

where

(a) $u(s,g,\omega,z=0)$ are the given initial values.

(b) The plus or minus sign is set according to whether one wants
     to propagate forward or backward in time.

(c) The velocity v can vary arbitrarily in the horizontal (s,g)
     or vertical (z) directions.

Now equation (1), along with the initial values $u(s,g,\omega,z=0)$, can generate the three-dimensional wave field $u(s,g,\omega,z)$ in which ω is held constant. A simple physical picture can be gained if equation (1) is solved by splitting: that is, alternatively applying the equations

$$\frac{\partial u}{\partial z} = \pm i \frac{\omega}{v} \left[1 + \frac{v^2}{\omega^2} \partial_{ss} \right]^{\frac{1}{2}} u \qquad (2)$$

$$\frac{\partial u}{\partial z} = \pm i \frac{\omega}{v} \left[1 + \frac{v^2}{\omega^2} \partial_{gg} \right]^{\frac{1}{2}} u \qquad (3)$$

to continue u downward in z by steps of Δz . These equations are identical to the regular one-way operators of the scalar wave equation. Equation (2)

represents the downward continuation of a common-geophone gather, and equation (3) represents the continuation of a common-shot gather. This is the familiar picture given above of achieving migration by alternately continuing the shot and receiver fields.

Without boundaries, the DSR equation is separable: one could propagate the shots down to the full depth z with (2), then subsequently continue the geophone field down with equation (3). In either case -- splitting or separation -- the solution would be the same. However, with an arbitrarily shaped boundary in the shot-geophone plane, (1) is not necessarily separable. This may have an effect on how well the migration behaves with certain boundary conditions -- in particular, absorbing boundary conditions.

The imaging condition for pre-stack migration is the same as that for normal zero-offset migration: t = 0. Any downward-continued geophones that receive scattered energy at zero time must be coincident with the scatterer; likewise the downward-continued source illuminating the scatterer must be at the scatterer's location. The imaged wave field u(s=g,t=0,z) is the sum over frequency of the separately propagated fields:

$$u(s,g,t=0,z) \; = \; \sum_{\omega} u(s,g,\omega,z) \tag{4}$$

In addition, all the coherent energy from reflection events is expected to concentrate on the zero-offset section, where shot and geophone are coincident. This presents the interesting possibility that non-focusing noise may be discriminated against in shot-geophone migration.

The imaging conditions s = g and t = 0 reveal that shot-geophone migration is a combination of the operations of migration and stacking. Also this particular form of the DSR equation produces a migrated depth section, in contrast to a migrated time section.

There is one more important point concerning imaging. To realize the correct imaging of the data, the correct velocity function must be supplied. No implicit velocity estimates are made in this procedure, and an incorrectly determined velocity will either underfocus the data or overfocus it. Examples of migrations performed with differing velocity functions are shown later.

Algorithms

The algorithms for modeling and migrating the shot-geophone experiment each comprise two major functions: propagation and imaging. Given a velocity model and an arbitrary scattering model, the modeling algorithm generates a synthetic set of common-shot gathers (or, common-geophone gathers). The "imaging" principle in modeling is to feed the scatterers into the wave field at zero time and zero offset as the wave field is propagated upward to the surface z=0. The imaging principle of migration is the opposite: extract the wave field at zero time and zero offset as the wave field is propagated downward. The only difference in the propagation sections of the algorithms is a change in sign of the frequency ω. Modeling projects the wave field forward in time while migration projects it backward in time. Other than the change in sign, the propagation operators employed are identical in the two cases.

Migration ---

Input: $u(s,g,\omega)$ at $z = 0$.
          $v(x,z)$ velocity model, where $x = s$ or g.

Output: Various outputs are possible,
   (a) $u(s,g,\omega,z_0)$ for some depth z_0.
   (b) $u(s,g,t=0,z)$ all offsets migrated.
   (c) $u(s=g,t=0,z)$ zero-offset migrated depth section.

   Read in $v(x,z)$
   Zero out scattering field $s(x,z)$
   For each frequency ω,
   | Read in shot-geophone plane $u(s,g,\omega,z=0)$
   | For each z level,
   | | Propagate:
   | | Downward continue common-shot gathers by Δz
   | | Downward continue common-geophone gathers by Δz
   | | Image:
   |__ |__ Add $u(s=g,\omega,z)$ to $s(x,z)$
   Write out $s(x,z)$. This represents $u(s=g,t=0,z)$

Modeling ---

Input: v(x,z) velocity field, where x = s or g

         s(x,z) scattering field (the reflectors)

Output: u(s,g,ω,z=0)

     Read in v(x,z)

     Read in s(x,z)

     For each frequency ω,

             Zero out u(s,g,ω,z) at depth z = maximum

             For each z level,

                 Image:

                 Add s(x,z) to the diagonal u(s=g,ω,z)

                 Propagate:

                 Upward continue common-shot gathers by Δz

                 Upward continue common-geophone gathers by Δz

             Save u(s,g,ω,z=0) at the surface

   For the examples that follow, all floating point arithmetic was done in an array processor controlled by our host machine. A basic requirement of this algorithm is that the entire shot-geophone field for a single frequency be stored in the memory of the array processor. In this way, repeated transposes of the shot-geophone plane are not necessary -- all common-shot traces and common-geophone traces are resident in the array processor and can be operated on *in situ*. Additionally, it is convenient if the velocity and scattering fields, v(x,z) and s(x,z), can likewise be held inside the array processor, but this is not absolutely necessary. If they cannot be held, the number of disk-to-array-processor transfers increases. In this case the number of transfers needed is about 2*nw*nz/iz, where nw is the number of frequencies, nz is the number of depth steps, and iz is the number of depth steps that can be done contiguously before a disk transfer is required. The size of each transfer is of course the number of complex values in the shot-geophone plane for a single frequency.

Operation Count:

The length of the downward-continuation operator is equal to the number of traces in a gather. The total number of downward continuations performed is nw * nz * nr * 2 where nw is again the number of frequencies, nz the number of depth steps, and nr is the number of gathers. It should be noted that the operation count is independent of the number of disk transfers required.

Operator:

The 45-degree approximation to equations (2), (3) was used as the downward-continuation operator for shots and geophones. Dip filtering has been incor-porated in order to remove artifacts that are present with the standard 45-degree operator. For a description of the operator see Jacobs et al. (SEP-16, p.89).

Data Preparation:

The migration algorithm requires that the input wave field be in the temporal frequency domain. Therefore to prepare the data for shot-geophone migration, the following steps must be taken:

(a) Fourier transform each field trace t to ω.

(b) Transpose the dataset so that frequency is the slowest varying parameter. The data is then organized into a series of shot-geophone planes indexed by ω.

(c) If the shot spacing happens to be different from the geophone spacing, or for any irregular shooting geometry, the shot-geophone field must be interpolated onto a regular grid where the shot interval is equal to the geophone interval. This involves a two-dimensional interpolation.

Once these operations are made, they need not be repeated -- migrations with various velocity models may start with the modified file.

Absorbing Boundaries:

In working on a finite grid in the spatial shot-geophone domain, it is

important to suppress the unwanted reflections which are generated at the grid boundary. Either a padded region must be added, which may increase storage requirements to the point of rendering the migration impractical, or absorbing boundary conditions must be employed. In the examples that follow, even with "standard" absorbing boundaries built into the operator, there are still substantial reflections off the grid edges. This may be due to the fact that the initial value problem is no longer separable when a finite boundary is placed around the shot-geophone plane. Figure 1 shows the boundaries of the discrete shot-geophone plane used in the examples of this paper. The boundaries were intentionally set so that the process of downward continuing shots would be symmetrical with downward continuing geophones. Two types of boundary are seen on figure 1: edges that are parallel to an axis, and edges that are diagonal to the axes. Now on the diagonal boundary it may happen that the two boundary conditions applied at one point (one in the shot direction and one in the geophone direction) are inconsistent with each other. For example, in order to satisfy a zero-slope boundary condition in both the shot and geophone directions, the wave field may have to be identically constant. Boundary conditions could be designed that involve terms in s and g, but these conditions together with equation (1) would make the problem inseparable. The likely answer is to use a split version of an absorbing boundary condition involving z, s, and g, in the same way that (2) with (3) is a splitting of equation (1).

Examples of Shot-Geophone Migration

The common-shot gathers of the following examples were generated synthetically with the modeling algorithm described above. These synthetic "field experiments" were migrated in turn with various velocity models. It can be seen that for all models, when the correct velocity is applied to the migration, a good imaged section matching the original reflectivity model is obtained. This merely demonstrates that the algorithm is reversible. Even the grid edge reflections are migrated in the proper way so that they "undo" themselves and contribute to the imaged section. The problem of missing data is not present in these synthetic examples as it is for real data. Nevertheless the examples show how sensitive the results of pre-stack migration may be to the prescribed velocity function.
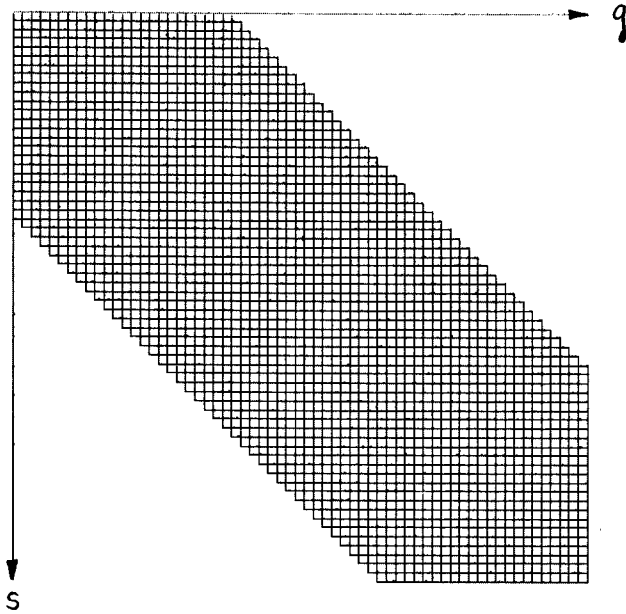
FIG. 1. The discrete shot-geophone plane. This is the actual size of the grid used in making the examples.

All of the examples were run with the following parameters:

nq = number of traces per gather   = 48

nr = number of gathers (shot or geophone) = 64

nz = sample points in depth   = 64

nt = sample points in time   = 64

Δs = shot interval = group interval   = 30 m

Δz = depth interval   = 15 m

Δt = time interval   = 0.025 sec

Therefore, time sections are 1920 meters by 1.6 seconds and depth sections are 1920 meters by 860 meters vertical. Notice that the depth sections are compressed in the horizontal direction by a factor of 2.

Model 1 -- Impulse Response in a Constant Velocity Medium

A single point scatterer lies 240 meters beneath the surface at the center of the seismic line. The velocity used to generate the synthetic data is a constant 2000 meters/second.
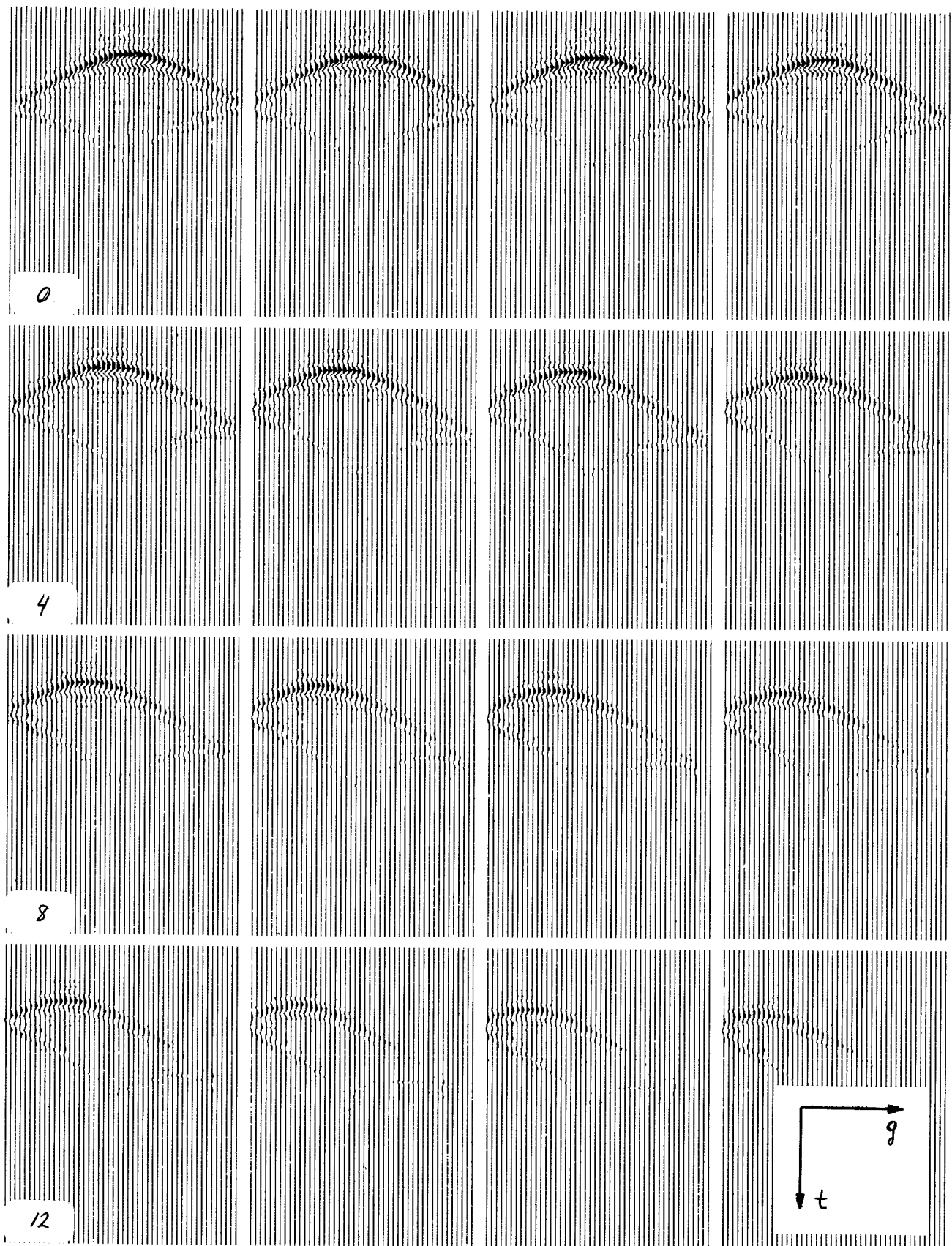
FIG. 2. Common-shot gathers 0-31 for model 1, a point scatterer in a constant-velocity medium. Gather 0, in the upper left corner, corresponds to the shot directly over the scatterer. The higher-numbered gathers correspond to the scatterer progressively shifted to the left with respect to the shot. The scatterer lies at a depth of 240 meters. Each gather is a time section. The edge reflection is obvious in these figures. In figure 3, it takes on the appearance of an event below the true scattered event.

FIG. 2. Continued.

midpt

t
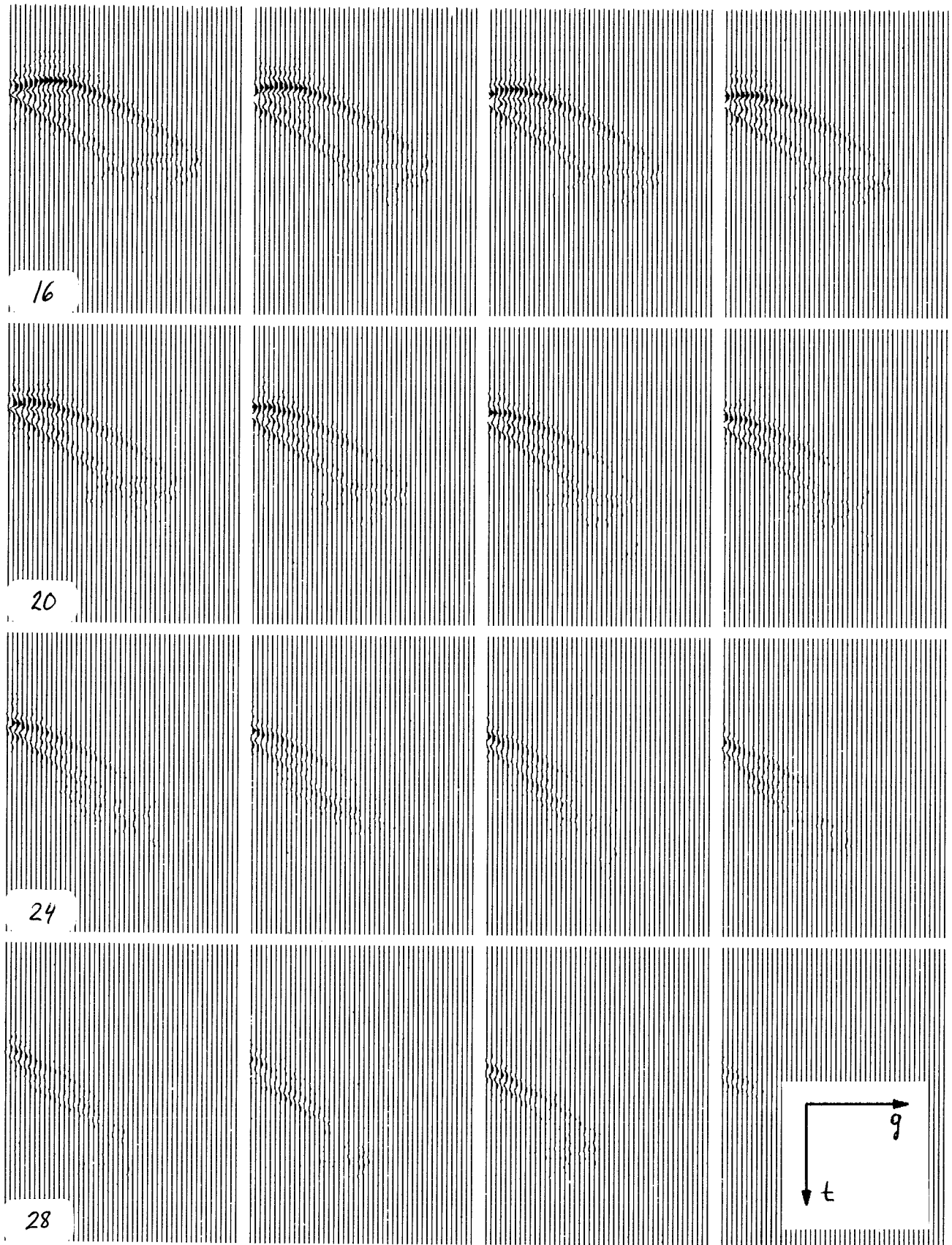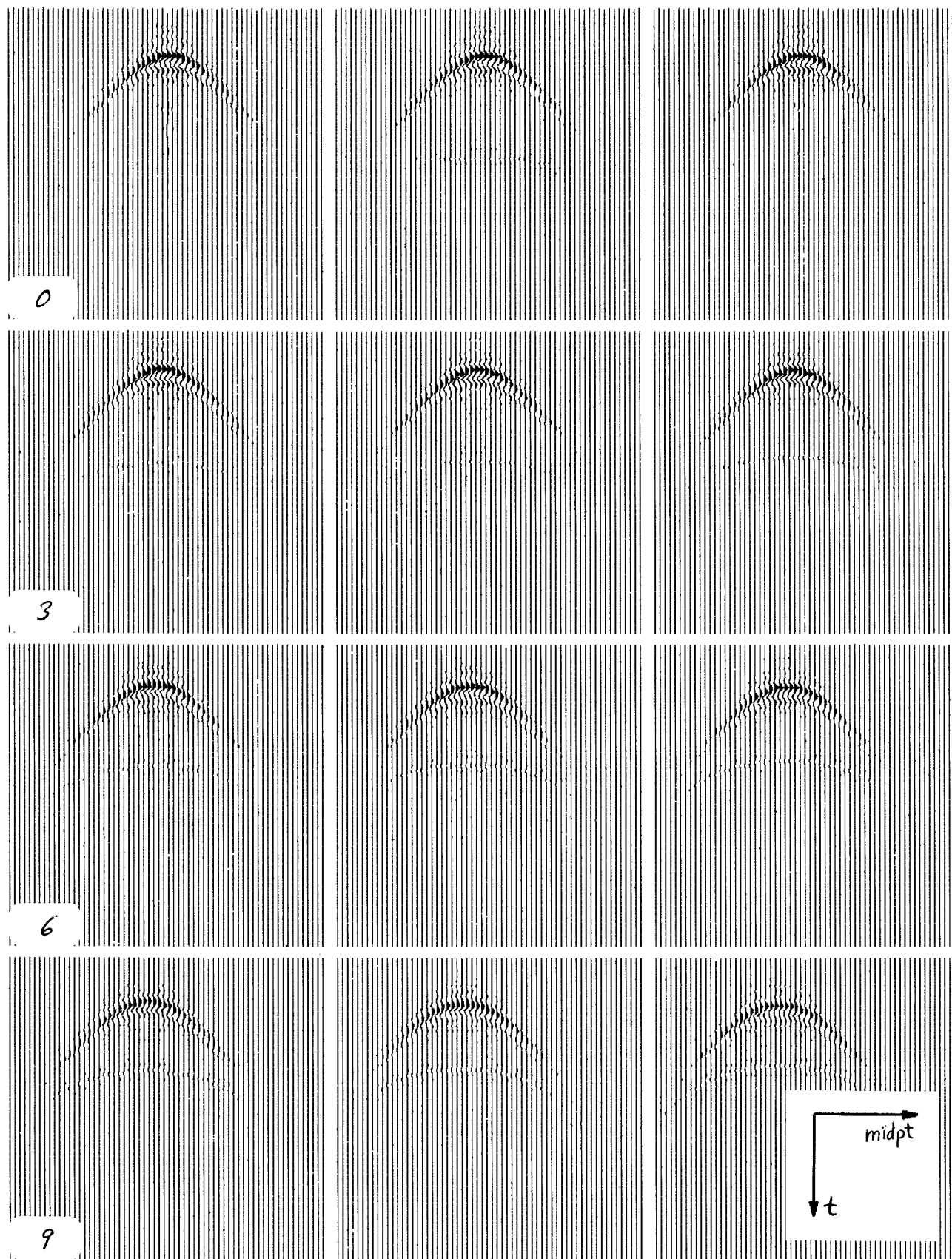
FIG. 3. Common-offset sections 0-23 for model 1. Offset number 0 is the zero-offset section, which displays a hyperbolic response. Greater offsets exhibit flattening on top of the moveout curve. Also present on the far-offset sections are events corresponding to the reflections off the diagonal boundary of figure 1. At the farthest offsets they merge into the real events as the diagonal boundary is approached.

12

15

18

21

midpt

t
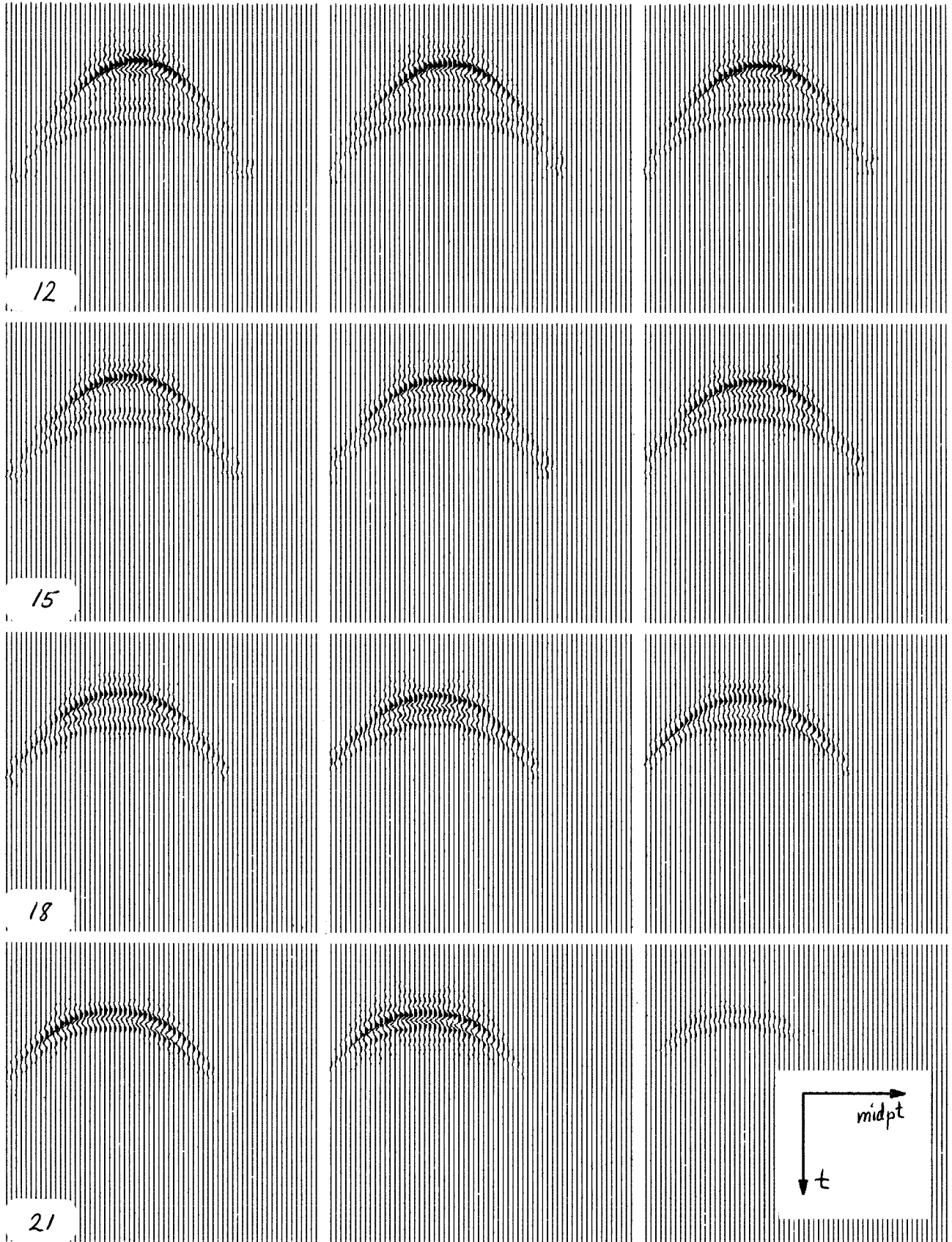
FIG. 3. Continued.

Fig. 2 -- Common-shot gathers generated by this model.

Fig. 3 -- Common-offset time sections generated by this model.

Fig. 4 -- Migrated zero-offset depth section using the correct velocity.

See the figure captions for details. The shape of the impulse response is as expected -- a hyperbola -- even out to far offsets. The unwanted edge reflections manifest themselves very plainly in figures 2 and 3, especially in the far-offset sections of figure 3.
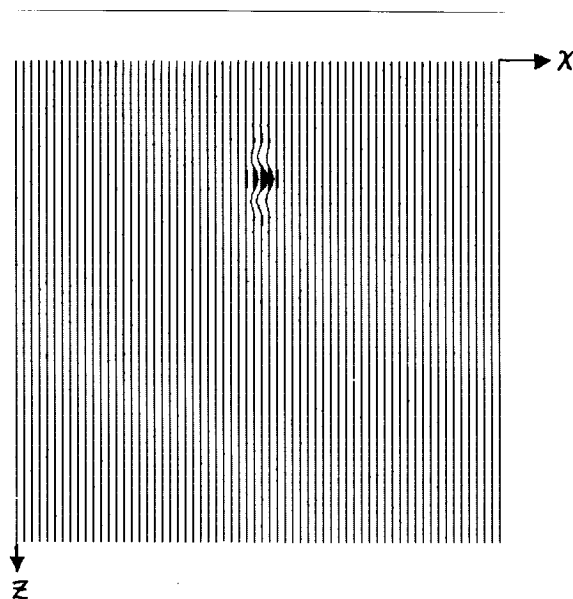
FIG. 4. Migration of the data of figures 2 and 3. The horizontal axis is midpoint x, vertical axis is depth z. Good resolution is obtained in the midpoint direction. The edge reflections have collapsed back into the scatterer, and so have contributed to the focusing effect. The original depth of the scatterer is 240 meters, the depth to the bottom of the section is 860 meters.

Model 2 -- Flat Reflector Beneath a High-Velocity Wedge

A flat reflector (figure 5a) underlies a wedge of higher-velocity material (figure 5b). The resulting synthetic dataset (figure 6) is not surprising: a gradual pull-up in time toward the right as the rays encounter a thicker portion of higher-velocity material. There is no apparent curvature to the reflector on the time sections -- it remains linear. This synthetic dataset was migrated using two velocity functions. First, the original

18

velocity function (figure 5b), and second, a constant velocity function of 2000 m/sec. The results are again what is to be expected: the correct velocity images the true reflector, while the constant velocity case results in an image of an evenly dipping layer. The focusing in this second case is rather good, so the misapplied velocity does not affect the quality of the image in this case, but only the placement of the image.

Fig. 5 -- Reflectivity and velocity fields, model 2.

Fig. 6 -- Common-offset gathers of the synthetically generated data.

Fig. 7a -- Correctly migrated zero-offset section.

Fig. 7b -- Incorrectly migrated zero-offset section.
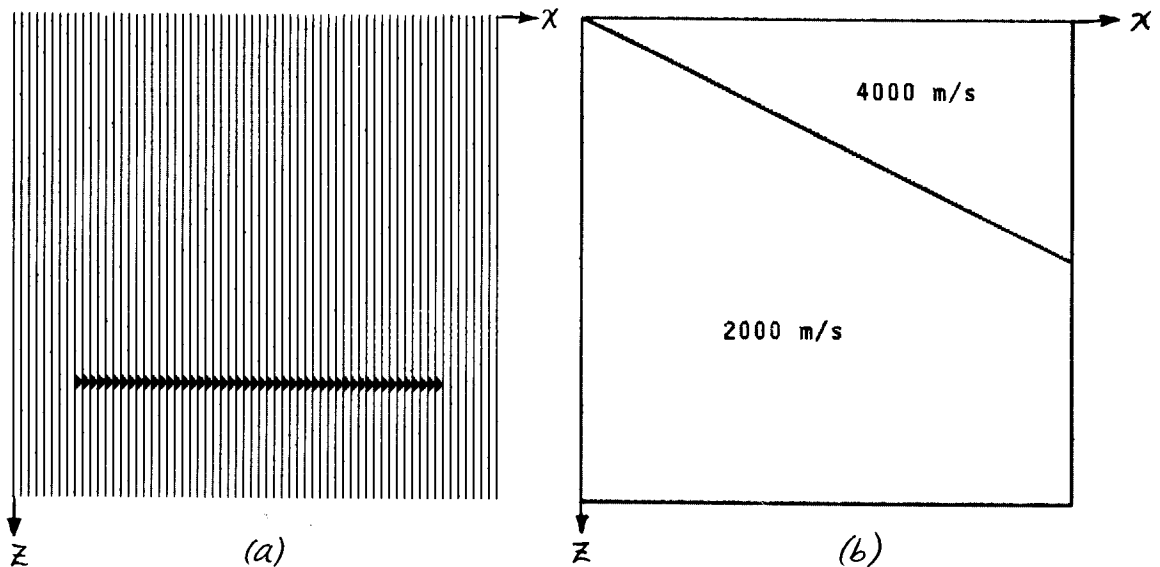
FIG. 5. (a) Reflectivity field for model 2. A flat reflector (i.e. a composi-
tion of point scatterers) lies at a depth of 720 meters. (b) The velocity
model. It is a wedge of 4000 m/sec material overlying 2000 m/sec material.
Observe that the velocity model is used purely for one-way propagation of the
wave field. It does not give rise to any reflected energy at the linear inter-
face between 4000 m/sec and 2000 m/sec.
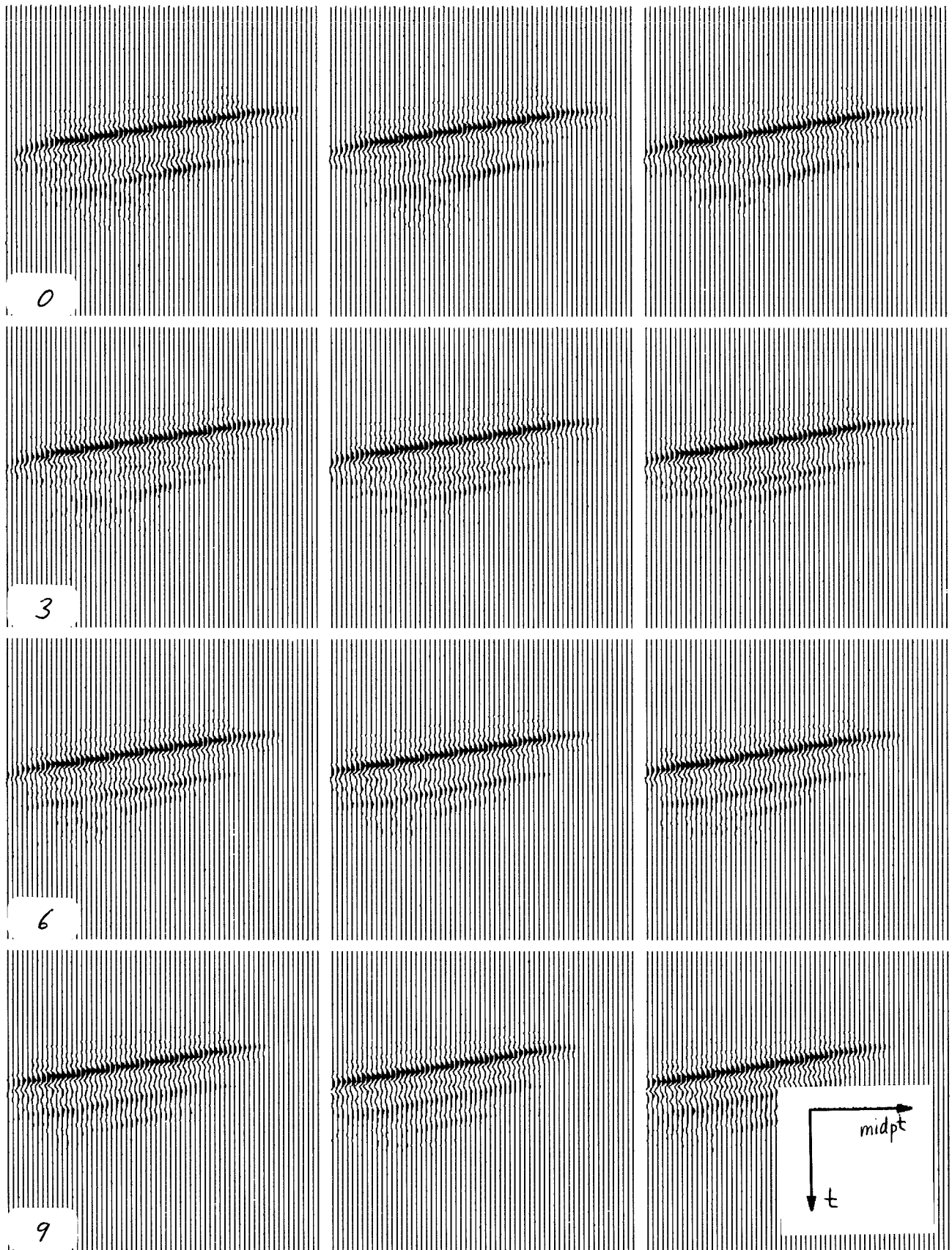
FIG. 6. Common-offset sections 0-11 for model 2. This figure displays the
first 12 offsets out of a total of 24 offset sections. Zero offset is at upper
left. The primary effect of the high-velocity wedge is a uniformly increasing
pull-up of the reflector in time. There is no noticeable curvature to the
event. The events beneath the reflector are grid reflections off the diagonal
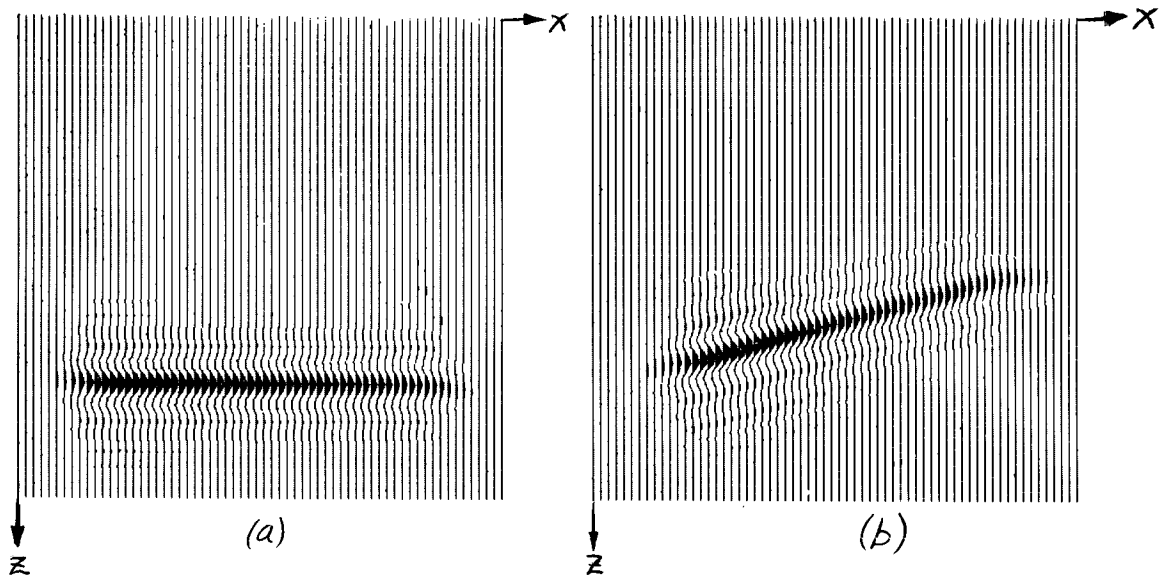boundary of the shot-geophone plane.

FIG. 7. Depth migration of the data of figure 6, using two different velocity
field inputs. (a) is by the correct velocity model (figure 5b) while (b) is by
an incorrect velocity model: the velocity is a mere constant 2000 m/sec. The
high-velocity wedge has produced an effective linear pull-up to the reflector
which a constant velocity function cannot correct for. Both figures (a) and
(b) are zero-offset depth sections.

Model 3 -- Dipping Bed in a Constant-Velocity Material

The previous model invites a comparison to the case of a dipping bed
(figure 10a) in 2000 m/sec material. The constant-offset sections (figure 8)
look very similar to the constant-offset sections of model 2 (figure 6). In
fact, if a migration is made using the velocity field of model 2, that is, the
high velocity wedge over a lower velocity, one obtains an imaged reflector
whose dip has been removed. In this case, though, the dip of the reflector
happened to be real. This demonstrates an ambiguity between models 2 and 3:
two datasets are virtually identical for two different physical cases.

Fig. 8 -- Constant-offset time sections of model 3.

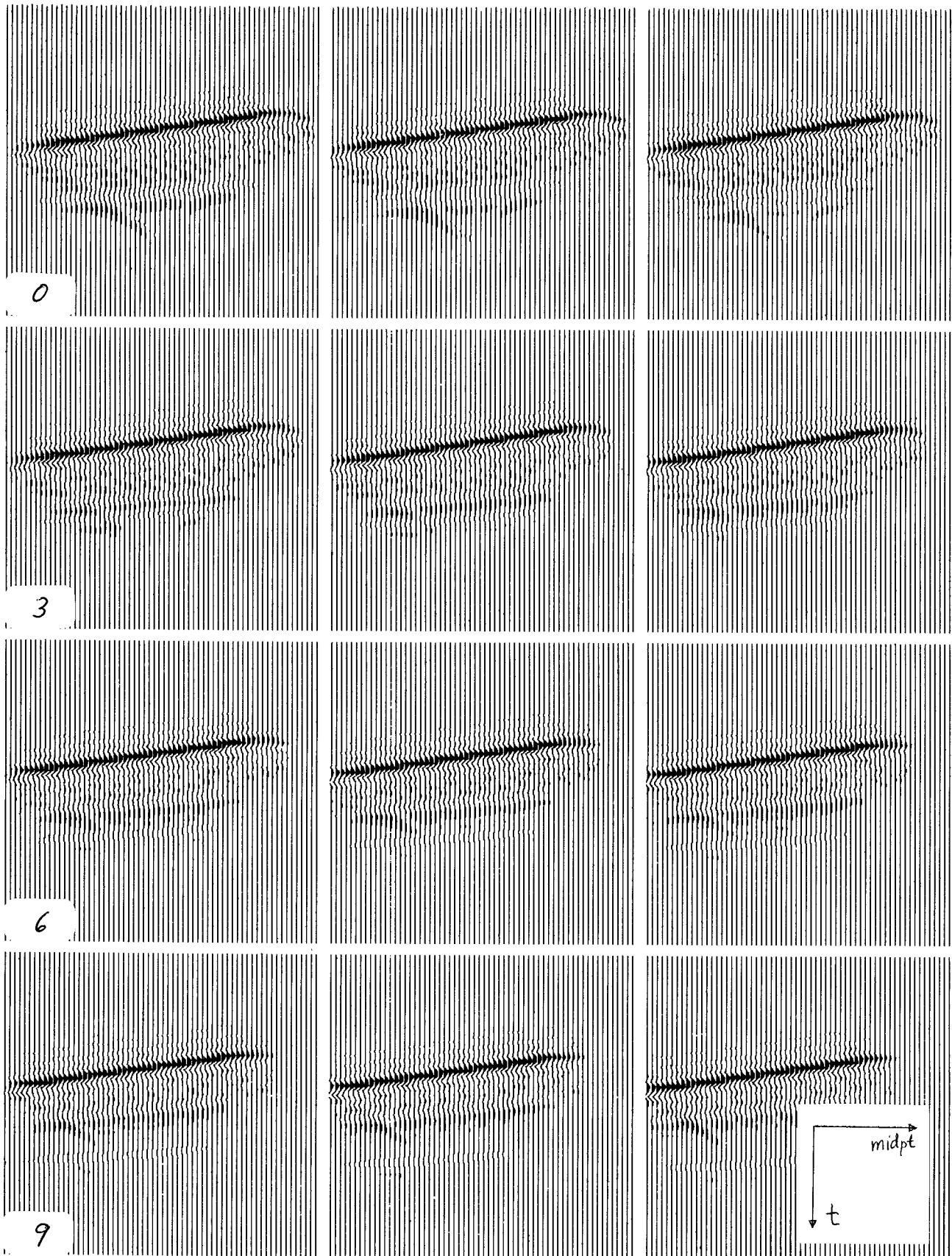Fig. 9 -- Incorrectly migrated zero-offset depth section.

midpt

t

FIG. 8. Common-offset sections 0-11 for model 3. Zero-offset is at upper left. This figure should be compared to figure 6. There is virtually no difference in character between the datasets of model 2 and model 3.
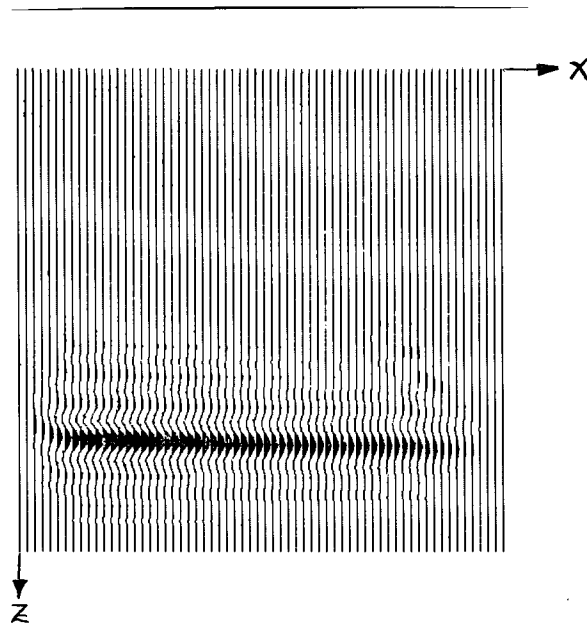
22

FIG. 9. The data of figure 8 was migrated using the wedge velocity model of figure 5b. The result is no different from the correctly migrated section (figure 7a) of the previous model.

Model 4 -- Dipping Bed Beneath a Low-Velocity Channel

The reflectivity model used to generate this dataset is the same as that for model 3 -- a dipping bed. But the velocity model now used has sharp lateral discontinuities, so that the synthetic data (figures 11 and 12) now appear somewhat complex. The migrated volume $u(s,g,t=0,z)$ using the correct velocity function (figure 10b) is displayed in the form of common-offset sections and common-midpoint gathers (figures 13, 14). The correctly imaged section, as expected, lies on the zero-offset section. Three other velocity functions were tried in migrating the synthetic model. For each case, the zero-offset depth section and the fourth-offset depth section (corresponding to an offset of 240 meters) is plotted. For the first trial velocity, the channel of 1000 m/sec material is replaced with 2000 m/sec material (figure 15a). For the second, a smoothed averaged velocity model is tried (figure 16a). For the third, an average velocity function is tried that matches more closely the true velocity -- one that has abrupt lateral discontinuities. Only the third trial is able to migrate the data reasonably so that it focuses well into a single event, though timing is off.

Fig. 10a -- Reflectivity field for model 4.

Fig. 10b -- Velocity field for model 4.

Fig. 11 -- Common-offset sections of the synthetically generated data.

Fig. 12 -- Common-midpoint gathers of the synthetic data.

Fig. 13 -- Common-offset sections of correctly migrated data.

Fig. 14 -- Common-midpoint gathers of correctly migrated data.

Fig. 15 -- Common-offset migrated sections using trial velocity 1.

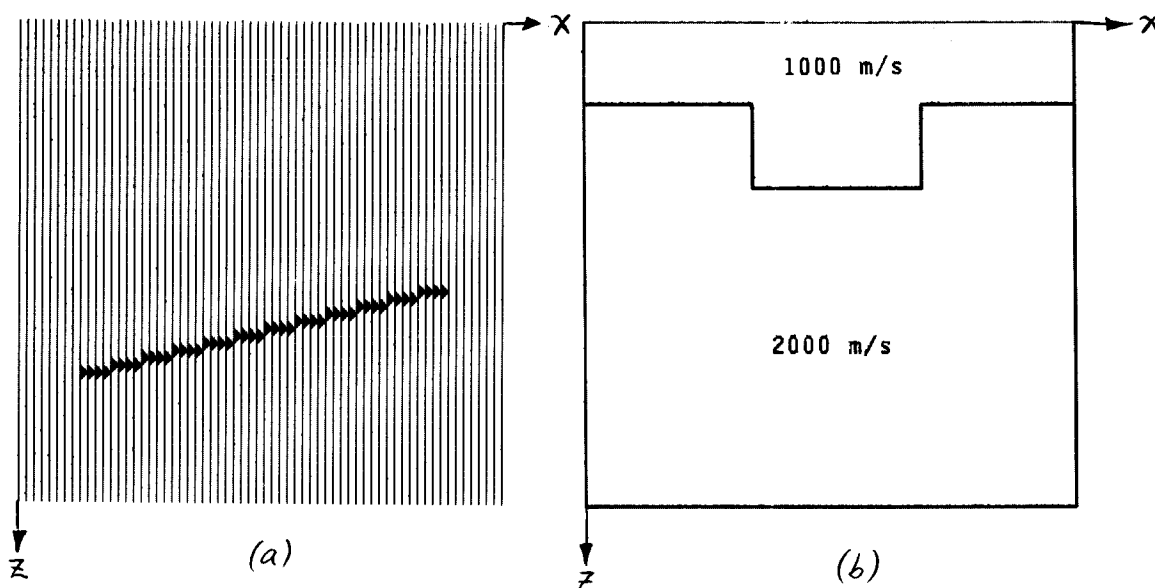Fig. 16 -- Common-offset migrated sections using trial velocity 2.

Fig. 17 -- Common-offset migrated sections using trial velocity 3.

FIG. 10. (a) Reflectivity model used to generate model 4 -- a dipping bed. (b) The velocity function used to generate model 4. It is an idealized low-velocity trough with vertical sides. The depth to 2000 m/sec material is 140 meters on the side and 280 meters in the center of the model.

A measure of how well the migrated section has been imaged is the ratio of energy of a certain reflector on the zero-offset section to its energy on a non-zero-offset section. The following table gives this ratio between offset zero and offset four for each of the trial velocities in figures 15, 16, and 17, as well as that for the correctly migrated dataset (figure 13). The correctly migrated set of course has the most effective imaging. The measure

of "energy" here is the maximum amplitude on the reflector in the common-offset section.

```
Trial velocity 1:    .097/.066  =  1.47
Trial velocity 2:    .103/.079  =  1.30
Trial velocity 3:    .129/.067  =  1.93
Correct velocity:    .129/.049  =  2.63
```
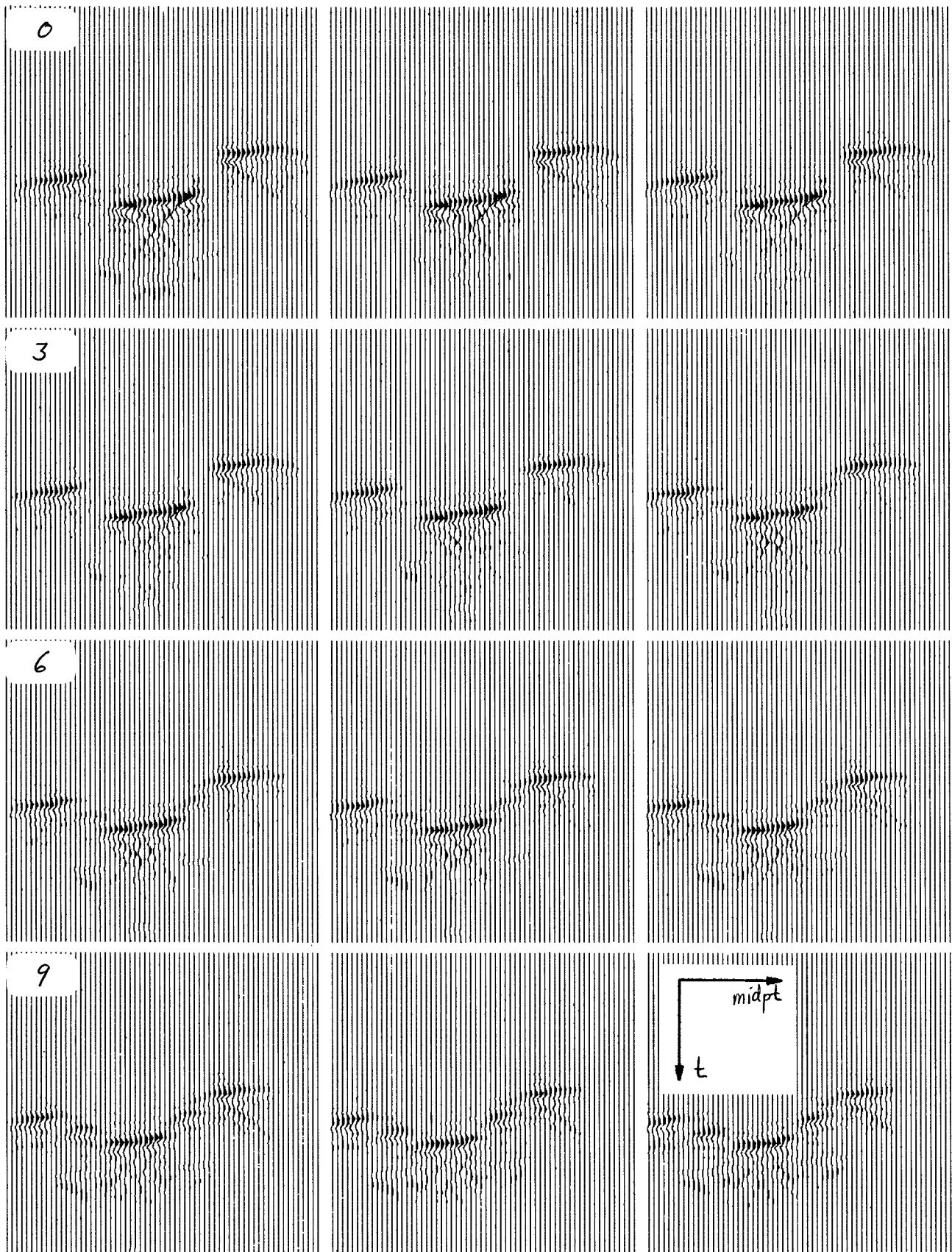
FIG. 11. Common-offset sections 0-23 for model 4 -- a dipping reflector beneath a low-velocity trough. Multiply the offset number by 60 to get the offset in meters between shot and geophone for each section. The zero-offset section (upper left) is understandable: the reflector is pulled down in time by the lower-velocity infill material. On the ends of the section the reflector is high, which corresponds to raypaths that miss the

26
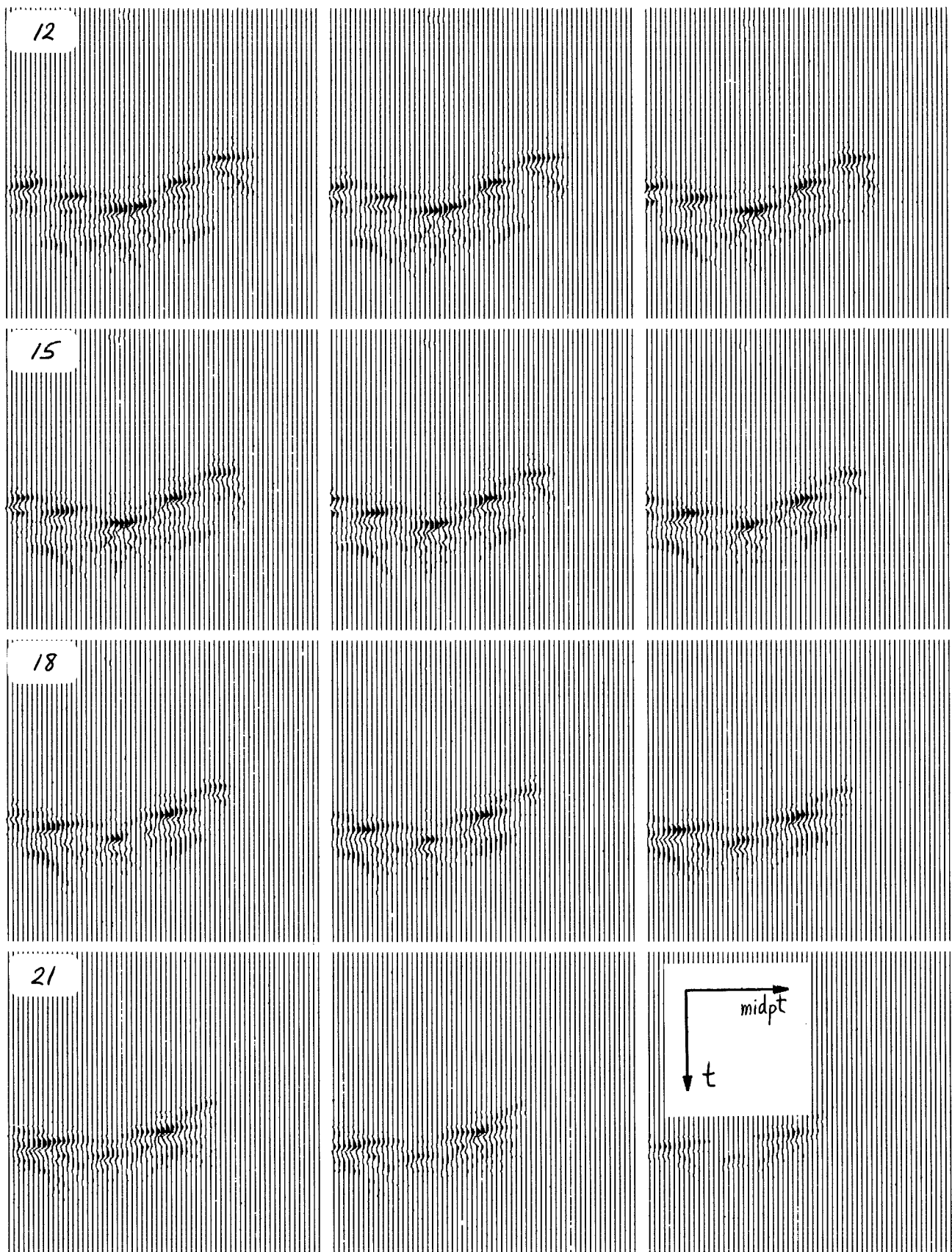
(FIG. 11. continued) low-velocity trough. On the large-offset sections an event appears midway between the normal arrival and the pulled-down arrival, and it corresponds to rays that travel through the trough region on the way down and miss it on the way up, or vice-versa. The three levels do not overlap significantly on the offset sections. They are also readily apparent on the common-midpoint gathers of figure 12. Time is the vertical axis on all sections.
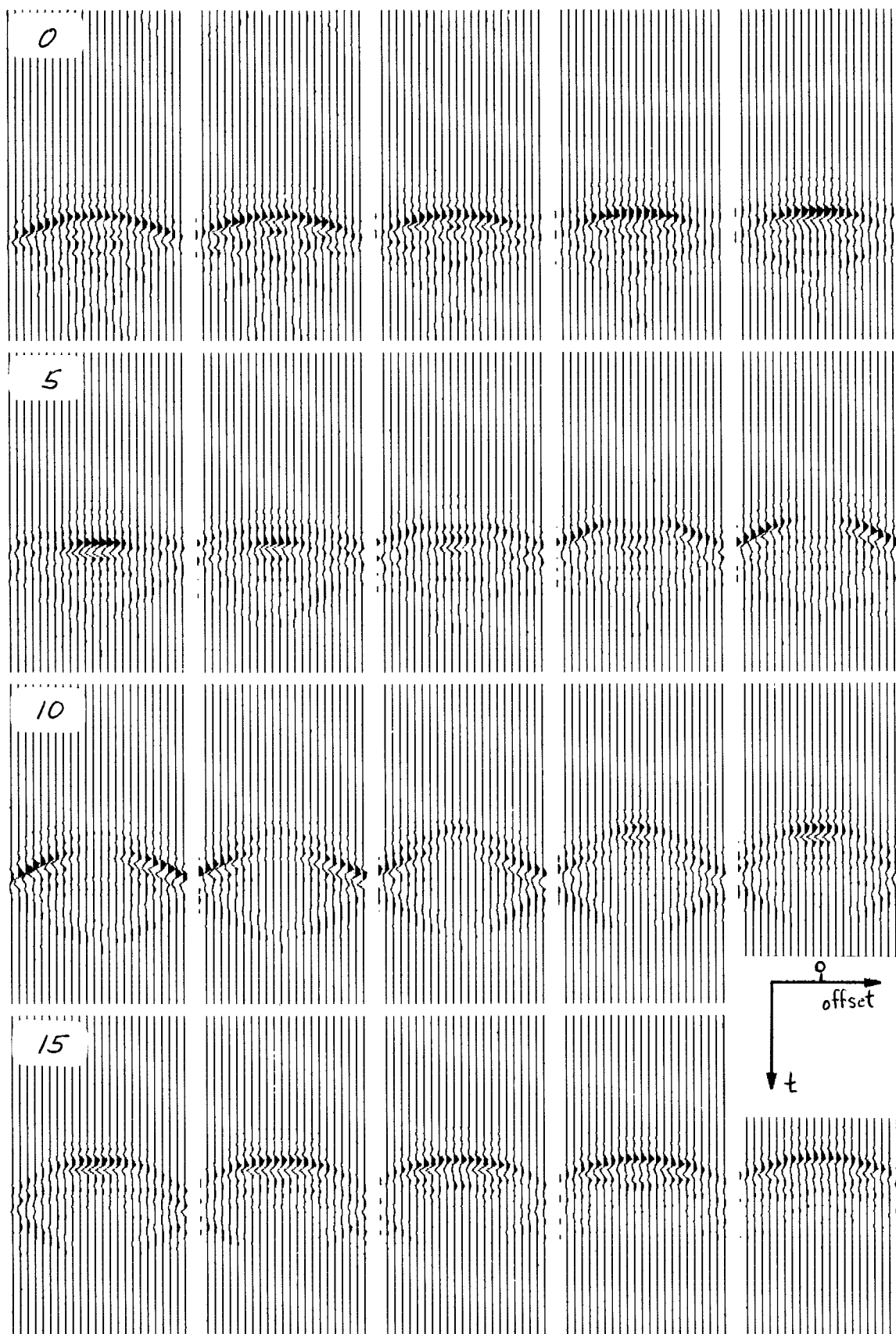
FIG. 12. Common-midpoint gathers 0-20 for model 4. See the caption for figure 11. The midpoint corresponding to the middle of the section is in the upper left corner. Increasing midpoints indicate gathers progressively updip on the reflector. Time is the vertical axis on all sections.
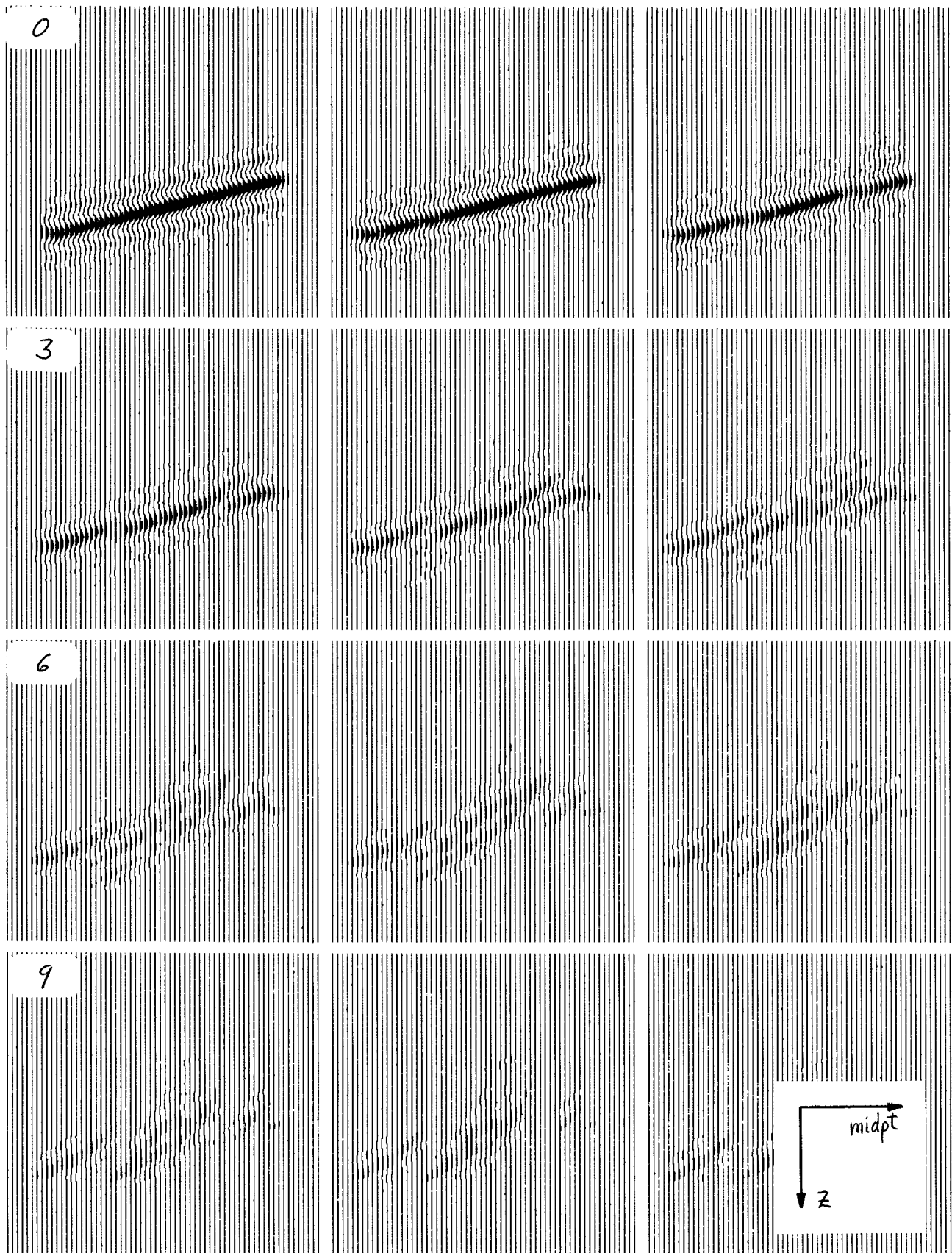
FIG. 13. MIGRATED common-offset sections 0-11 from model 4. Zero offset is in the upper left. The correct velocity function was used in the migration. The energy images correctly on the zero-offset section only. All sections are time sections. In contrast, figure 14 is a common-midpoint display of the same migrated set.
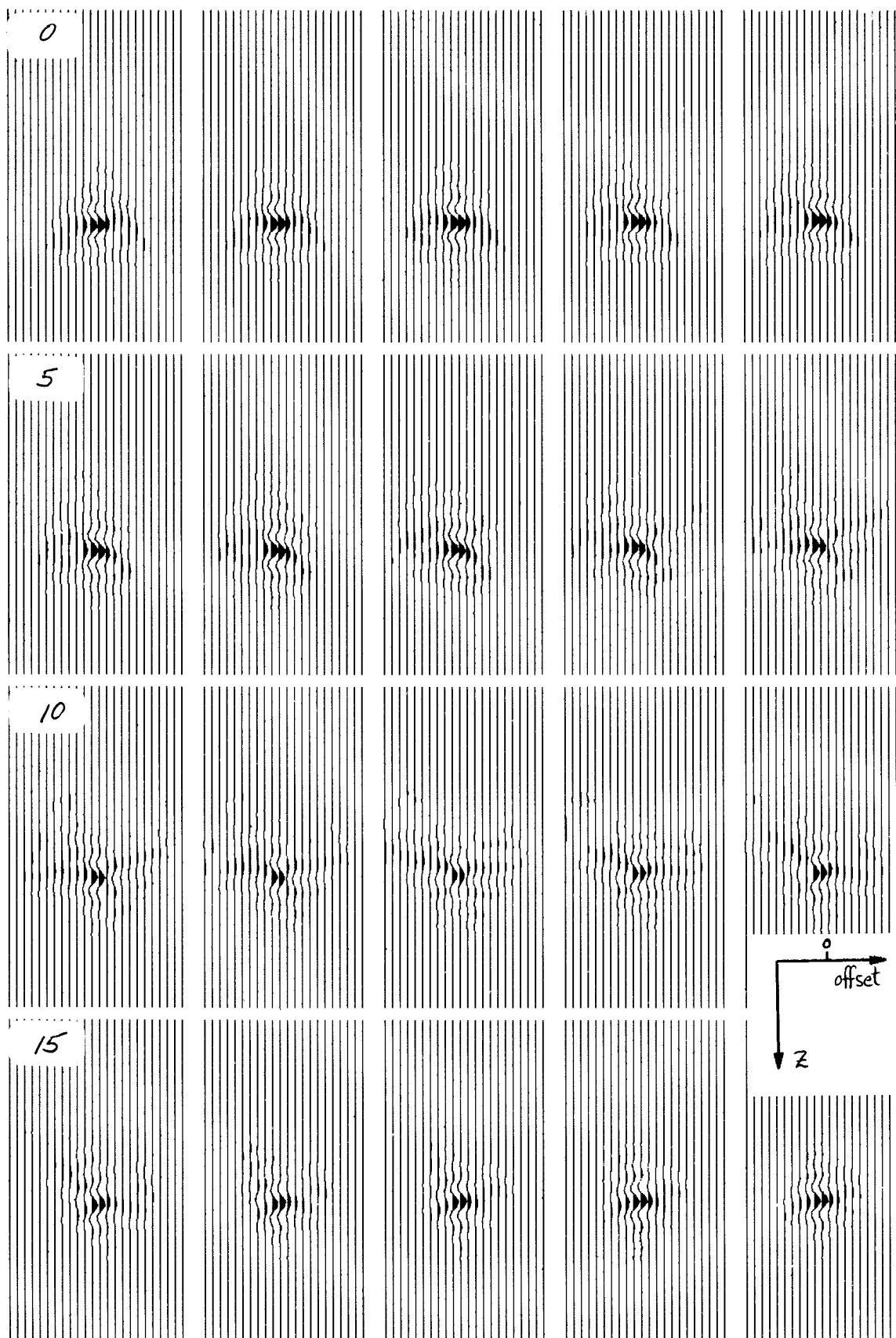
FIG. 14. MIGRATED common-midpoint gathers 0-20 for model 4. See the caption for figure 13. Overall energy has concentrated at the zero-offset section. This example seems to indicate that focusing resolution of the image in the midpoint direction is much greater than in the offset direction.
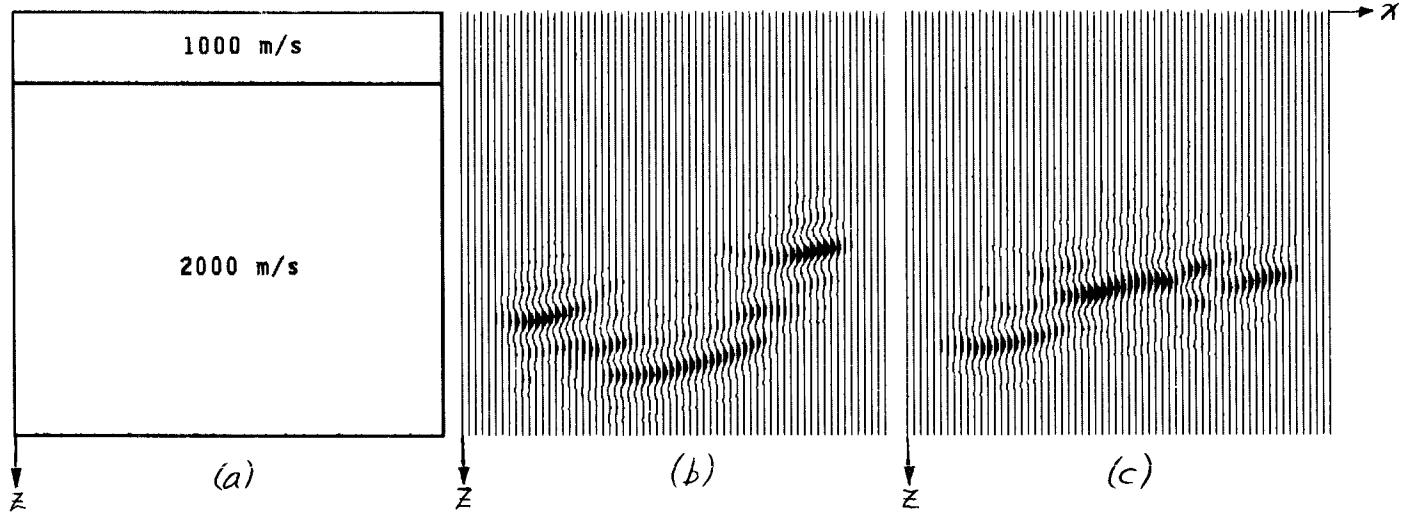
FIG. 15. The first trial velocity function used to migrate the dataset of figures 11 and 12 is simply the original velocity with the trough "filled in" with 2000 m/sec material. This does a poor job in imaging the data. (a) is the velocity model, (b) is the migrated zero-offset section and (c) is the migrated constant-offset section corresponding to an offset of 240 meters. The three events seen on figure 12 (due to the three possible types of raypaths through the material) do not coalesce in the imaged section as they do for the correct migration of figure 13. Sections (a), (b), (c) are in depth.
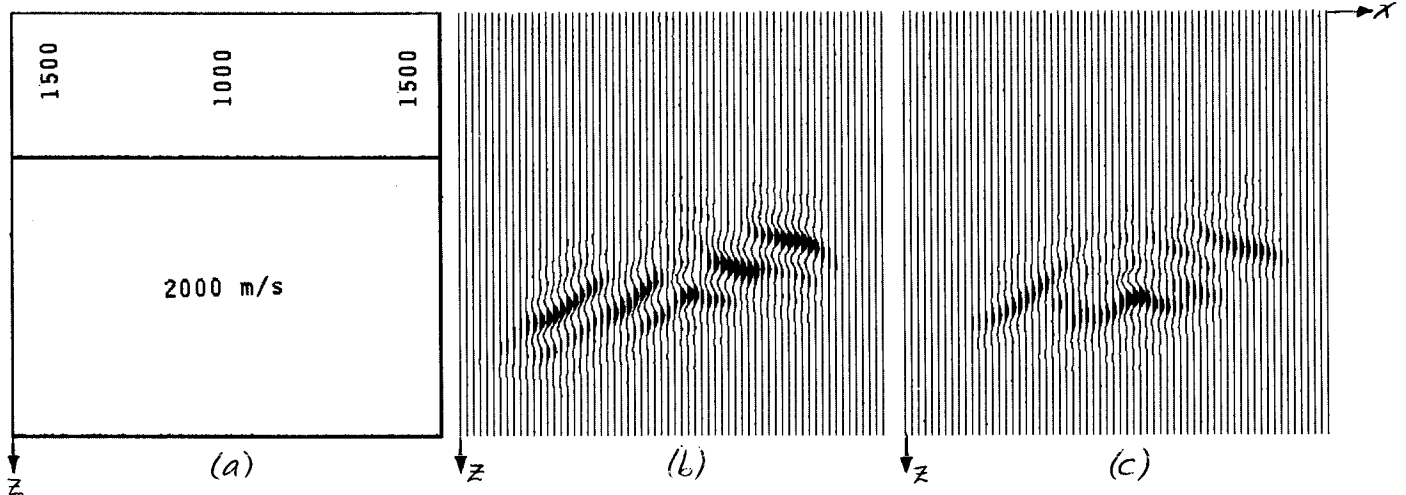

FIG. 16. Second trial velocity. The velocity model (a) here is a smooth laterally varying velocity in the shallow half of the depth section. (b) is the migrated zero-offset section while (c) is the migrated 320-meter constant-offset section. Again, when data which is generated by a velocity field with lateral discontinuities is migrated with a smooth laterally varying velocity, the multiple events do not image together properly. Sections (a), (b), (c) are all depth sections.
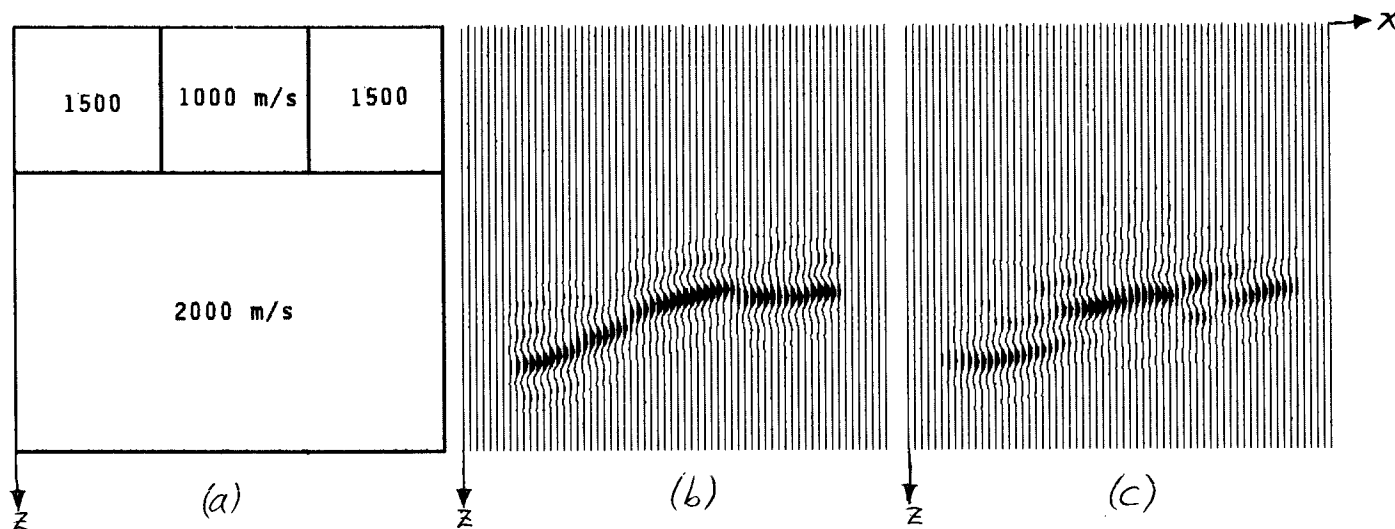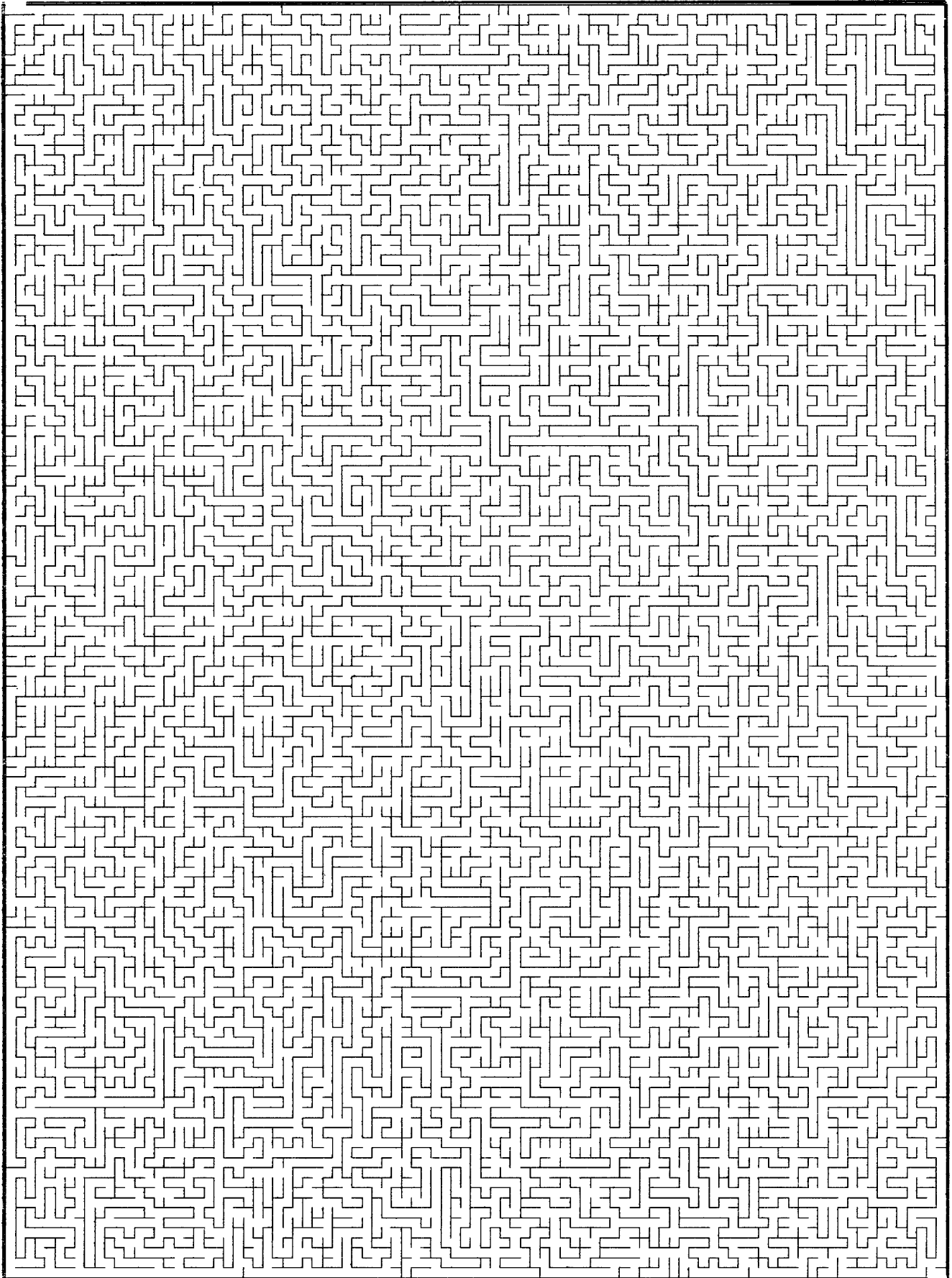
FIG. 17. Third trial velocity. The vertical average velocity of this model matches that of the true velocity field -- it has lateral discontinuities in the right places. (a) is the velocity model, (b) is the migrated zero-offset section while (c) is the migrated 320-meter constant-offset section. The reflector is imaged fairly well, except for an error in vertical position. All sections in this figure are depth sections.

IN

OUT

Solution on page 370.